Bulletin of the Seismological Society of America, Vol. 92, No. 4, pp. 1355–1364, May 2002

Coseismic Displacements from the Hector Mine, California, Earthquake: Results from Survey-Mode Global Positioning System Measurements

by Duncan Carr Agnew, Susan Owen, Zheng-Kang Shen, Gregory Anderson, Jerry Svarc, Hadley Johnson, Kenneth E. Austin, and Robert Reilinger

Abstract We describe the collection and processing of Global Positioning System (GPS) data from 77 locations around the Hector Mine earthquake, which we use to estimate coseismic displacements related to this shock. The existence of pre-event GPS data, some collected to monitor postseismic displacements from the 1992 Landers earthquake and some to establish survey control in the meizoseismal area, provided a relatively dense coverage close to the rupture zone. The data available were collected mostly within the 2 years prior to the 1999 earthquake; we reobserved many points within a few days after the shock, and all within 6 months after. We include corrections for interseismic motion to provide the best value possible for coseismic motion caused by this earthquake. The displacements in general display the pattern expected for a strike-slip fault, though a few show significant vertical motion. The maximum horizontal displacement observed was 2 m; one station between fault ruptures showed little horizontal motion, but significant uplift.

Introduction

Geodetic measurements of displacements from earthquakes began in California in 1857, with an (unsuccessful) attempt by W. E. Greenwell (Agnew and Sieh, 1978). The 1906 San Francisco earthquake led to the discovery of widespread displacements away from the fault (Hayford and Baldwin, 1908) and since then each large earthquake in California has been followed, sooner or later, by an estimate, from geodetic data, of the displacements it caused. Of course, as geodetic techniques have become more precise, the size considered large has diminished, and the amount of data available for a given size of event has increased.

This article represents the latest in this genre, for the Hector Mine earthquake of 16 October 1999. In particular, it follows the style of earlier reports on the 1992 Landers (Hudnut *et al.*, 1994) and 1994 Northridge (Hudnut *et al.*, 1996) earthquakes, in presenting a compendium of displacements derived from measurements using data from the Global Positioning System (GPS) that were collected in survey mode (also known as campaign data): that is, by occasional occupations of a survey monument with a GPS receiver. These are not the only measurements of coseismic displacements available for this earthquake, indeed not even the only GPS measurements. Coseismic displacements were also measured by the permanent GPS stations of the Southern California Integrated GPS Network (SCIGN); estimates of these displacements have been presented by the Hector Mine Earthquake Team (2000), by the SCIGN Analysis Committee (1999), and by Hurst *et al.* (2000). The SCIGN data cover a relatively restricted range of azimuths and do not extend close to the fault; the survey-mode data have much more complete spatial coverage, though also much less temporal resolution. In this article we document how the displacements of survey-mode points were estimated, especially given that these estimates involve corrections for interseismic motion that are unnecessary for the permanent GPS installations. Since the data reported here are only a part of the total dataset available for estimating static fault slip, a dataset that also includes very high-quality InSAR measurements (Sandwell *et al.*, 2000; Fialko *et al.*, 2001; Sandwell *et al.*, 2002), we have eschewed the custom of estimating a fault-slip model from the displacements.

Observations

Considerable high-precision GPS data had been collected around the area of the Hector Mine earthquake in preceding years, primarily to monitor postseismic deformations from the 1992 Landers earthquake (Shen *et al.*, 1994; Savage and Svarc, 1997), through surveys by universities (especially UCLA) belonging to the Southern California Earthquake Center (SCEC) and by the U.S. Geological Survey (USGS). Additional data were collected during control surveys of the California High-Precision Geodetic Network (HPGN), done by the National Geodetic Survey (NGS) and the California Department of Transportation (CADT). In addition, two sites close to the rupture (TROY and SIBE) and

several others more distant were occupied annually by Central Washington University (CWU) as part of a study of the Eastern California Shear Zone (Miller *et al.*, 2001). Except for the CWU measurements, all of these data had been archived at the SCEC Data Center as part of an effort led by three of us (Agnew, Johnson, and Anderson), so it was easy for us to find out quickly which stations could usefully be reobserved. Personnel from the USGS, from SCEC universities (USC, UCSD, and UCLA), and from CWU made the first such observations within 2 days of the earthquake; most points were reobserved within a week. The day after the earthquake, personnel from the Jet Propulsion Lab (JPL) set up continuously operating stations at TROY and SIBE; these sites are now part of SCIGN. The achieved data also showed a few points extending farther east and crossing the fault rupture; these had been observed in 1998 by UCLA to extend the Landers monitoring farther east. These points were located on the Air-Ground Combat Center (MCAGCC) of the U.S. Marine Corps (USMC); we resurveyed these as soon as this area was accessible, 6 days after the earthquake. Most of the points observed by USGS and SCEC personnel were reobserved at varying intervals thereafter to determine postseismic motion. In addition, personnel from the Massachusetts Institute of Technology (MIT) observed at a few additional points in early January 2000, mostly at locations more distant from the epicenter.

In early 2000 we learned of additional GPS data from the region close to the fault. In fall 1997 and spring 1999, members of the Meteorology and Survey Section, 11th Artillery, USMC, made low-precision surveys of a number of stations in and around MCAGCC to improve geodetic positions of points used for fire control. Given that even brief GPS occupations can provide positions good to a few centimeters, we felt it would be worthwhile to reoccupy as many of these points as possible close to the fault, and we did so as soon as they were accessible to us, in April 2000. We occupied all stations with prior GPS data that were within one rupture length of the fault; a few of these had been used earlier for postseismic monitoring.

Table 1 describes the points observed both before and after the earthquake; except for some more distant points, all these are shown in Figure 1. Table 1 gives the station code used, the location, and monument stamping (if any), and also gives the times of the last observation before the earthquake and the first one after it, along with the agency collecting the data. In a few cases data were available closer in time to the shock than is shown here, but these data were not used because they were less precise: for example, the USMC occupied station SAND in 1999, but we have used the earlier, more precise, data from the USGS.

Data Collection

All observations used dual-frequency GPS receivers. The SCEC data after 1996 and the USGS data after 1997 were all collected using Ashtech Z-12 systems with choke-ring antennas, matching the SCIGN installations. Most of the data collected by the CADT and the NGS utilized Trimble 4000SSE or SSi receivers. The USMC collected data with the Trimble MSGR, the military version of the 4000SSi equipment. While a variety of antenna types were used in these measurements, all were of designs for which phase maps relative to the choke-ring design are available. Much more important to the precision of the results is the duration of the observations. Most of the SCEC and USGS observations were for at least 8 hr, with many stations being observed continuously for several days. One exception was the SCEC stations observed in 1998 inside MCAGCC, which had durations of 4 to 6 hr. Most of the NGS and CADT observations were 5 to 6 hr in duration. The USMC surveys in 1997 and 1999, as appropriate for lower-precision GPS, had durations of 45 min; however, at a number of sites several such sessions would be observed in succession, making a total observation span of up to 3 hr, albeit with gaps in the data.

All survey-mode data from both before and after the earthquake, with the exception of the pre-earthquake data collected by CWU, are archived at the SCEC Data Center, *http://www.scecdc.scec.org;* the CWU data are archived at the PANGA Data Center, *http://www.panga.cwu.edu.* Data archived at the SCEC Data Center were converted to RINEX format if not already in that form and run through a suite of programs that merge information from the logsheets into the header of the RINEX file. Data for continuous sites was available in RINEX from the Scripps Orbit and Permanent Array Center (*http://sopac.ucsd.edu*).

Data Processing

We processed all data with the GAMIT (King and Bock, 2001) and GLOBK (Herring, 2001) processing packages. The solution used the survey-mode data for the day and data from 5 to 6 continuous stations across California, primarily from SCIGN.

In the first step, double-differenced phase data were used to solve for relative station positions, atmospheric zenith delays (every 2 hrs) and integer ambiguities. In this initial solution, we adopted the International GPS Service (IGS) satellite orbits with tight constraints, and also applied tight constraints to the positions of three regional SCIGN stations: MONP, BLYT, and PIN1. Once ambiguities were resolved, the software generated a solution with all parameters loosely constrained and a full covariance matrix.

The postearthquake data was processed for a full UTC day. Many of the pre-earthquake USMC data spanned the UTC day boundary; for these, the interval analyzed was limited to the span covered by the survey-mode data, and only the two closest SCIGN stations (PIN1 and GOL2) were included in the solution. Processing only this more local network made it possible to resolve more ambiguities for the relatively short spans of USMC data, which proved crucial

Table 1
Stations and Data Collection

ID	N Lat	E Long	Height	PID	Stamping	Last	First	Observers
0803	35.07183	−116.41459	512	FT1609	08-3 1	−629	83	UCLA/MIT
0808	34.72781	−115.93316	729	EU1246	08-8 1	−630	2	UCLA/SIO
6050	34.26607	−116.33408	834	AH5219	2838 19 DOR 1972	−693	2	UCLA/USC
6056	34.36963	−116.64714	911	EV2796	Q720 1944	−651	3	UCLA/UCLA
7000	34.67634	−116.71592	1178	AH5221	T7N R3E S19 S30 1919	−222	3	USMC/USC
7001	34.56002	−116.46923	802	AH5222	T6N T5E S32 S33 1919	−650	2	UCLA/USC
7002	34.36741	−116.40394	744		T3N 1/6/12/7 R5E R6E 1957	−2655	80	SIO/MIT
7007	34.70481	−116.22454	625		T7N R7E 10/11/15/14 LS 3579	−2650	2	Stanford/SIO
ACRN	34.33646	−116.32615	820		ACORN 2 SEP 98	−222	185	USMC/SIO
ADZU	34.35217	−116.24957	745		ADZUKI POLE II 1 NOV 1979	−746	185	USMC/USC
AIMR	34.43556	−116.34300	701		AIMERS	−222	184	USMC/SIO
AMBO	34.55863	−115.74249	163	EU0492	AMBOY 1934	−479	2	CADT/SIO
ANT_	34.48209	−116.38763	742		SCP ANT 6 DEC 78	−222	184	USMC/SIO
ARGO	34.73154	−116.25300	590	EV3952	ARGOS 1957	−222	187	USMC/USC
ASIA	34.39160	−116.28440	895		ASIA	−222	184	USMC/SIO
BAGJ	34.65528	−116.26385	717		BAGUIO APR 85	−229	186	USMC/UCLA
BAM2	34.45628	−116.28891	791		BAM II 9203	−746	186	USMC/USC
BEER	34.32513	−116.25665	718		BEER 1973	−221	185	USMC/SIO
BM52	34.68132	−116.32645	543		BM52LC 1953 1887	−229	184	USMC/UCLA
BRAY	34.45650	−116.26095	840		BRAY 2	−229	186	USMC/USC
CHUK	34.57081	−116.24358	885		CHUCK	−228	36	USMC/UCLA
CLR2	34.42912	−116.30616	1319		CREOLE NO 2 1934	−2630	66	USGS/SCIGN
CROS	34.72257	−116.11980	515	EV0839	CROSSING 1964	−743	187	USMC/USC
DODG	34.38378	−116.04103	763		DOD	−228	184	USMC/USC
DUMB	34.28803	−116.02762	678		DUMBELL	−227	184	USMC/USC
EAST	34.57787	−116.16200	676		EAST	−229	187	USMC/UCLA
EBON	34.49103	−116.17601	1084		EBONY	−227	208	USMC/USC
EDWI	34.55493	−116.09275	506		EDWIN 85/06/05	−228	187	USMC/SIO
ELEP	34.52273	−116.05611	477		ELEPHANT 85 06 05	−228	187	USMC/SIO
ELK1	34.44741	−115.86944	248		ELK 1973	−377	35	UCLA/SIO
END_	34.53060	−116.10198	578		END SEP 89	−228	187	USMC/SIO
GAYS	34.55499	−116.37858	974		GOOFY 1974	−746	42	USMC/UCLA
GHAZ	34.51335	−116.32618	879		BENGAZI	−746	43	USMC/UCLA
GODW	34.13642	−115.93156	505	EU0440	GODWIN 1965	−479	4	CADT/UCLA
GYPS	34.38551	−116.18248	718		GYPSUM	−227	185	USMC/SIO
HEBR	34.41151	−116.26302	913		HEBER	−221	185	USMC/USC
HECT	34.78498	−116.42070	597	EV3968	HECTOR 2 1966	−484	2	CADT/SIO
ISBO	34.33330	−116.14020	523		ISBO-1 1994 1821.84	−744	186	USMC/SIO
LAE1	34.57440	−116.55706	898		T6NR4E S28S27 1919	−621	1	USGS/USGS
LAE2	34.58891	−116.52205	910		T6NR4E S23S24S26	−621	1	USGS/USGS
LAE3	34.61794	−116.48682	935		T6NR15E S7S8S18S17	−622	1	USGS/USGS
LAE4	34.73414	−116.32917	613		T8NR6E S34S35 1974	−622	1	USGS/USGS
LAW1	34.54236	−116.58815	921		LAPW1	−619	1	USGS/USGS
LAW2	34.52669	−116.62369	915		3103 9 WBC 1976	−626	1	USGS/USGS
LAW3	34.50150	−116.66900	963		LAPW3	−619	3	USGS/USGS
LAW4	34.45383	−116.66521	854		2901 31 DOR 1972	−619	4	USGS/USGS
LAYZ	34.61042	−116.25293	787		LAZY	−229	186	USMC/UCLA
LAZY	34.34389	−116.51389	1027	EV9188	LAZY 1980	−480	2	CADT/USC
LEDG	34.50202	−116.43915	1169	EV3958	LEDGE 1935	−576	35	UCLA/SIO
LUCS	34.43949	−116.88193	885	EV0565	LUCERNE SOUTH BASE 1928	−595	6	UCLA/UCLA
LUDL	34.72322	−116.17570	509	EV3946	LUDLOW 1957	−743	187	USMC/USC
MAUM	34.41904	−116.45836	1238	EV4006	MAUMEE 1935	−576	35	UCLA/SIO
MCAL	34.33865	−116.32627	812		ALICE II MAR 89	−747	185	USMC/SIO
MCAN	34.37524	−116.35522	709		ANGLE	−222	184	USMC/SIO
MEAN	34.40479	−116.54970	1067	EV4007	MEANS 1935	−575	35	UCLA/SIO
MEEK	34.25791	−116.61743	1883	EV4009	MEEKS 1939	−621	6	USGS/USGS
MESQ	34.19327	−116.11342	611	EV3978	MESQUITE 1939	−693	2	UCLA/USC
OLDD	34.39050	−116.69794	941	EV0645	OLD 1935	−626	5	USGS/USGS
OLDW	34.38866	−116.75187	1198	EV4040	OLD WOMAN 1935	−578	6	UCLA/USGS
ONYX	34.19257	−116.70949	2749	EV4030	ONYX 1939 1982	−6	87	USC/MIT
PAXU	34.15311	−116.38982	1127	AG9879	PAX NCER 1977	−702	3	UCLA/UCLA

(*continued*)

Table 1
Continued

ID	N Lat	E Long	Height	PID	Stamping	Last	First	Observers
RAIN	34.97484	−117.20750	739		RAINBOW 1969	−483	3	CWU/CWU
RICU	34.26411	−116.46888	1279	EV4005	RICH 1939	−624	6	USGS/USGS
RVAL	35.14167	−115.40196	1575		3055 S	−483	5	CWU/CWU
SALY	34.44142	−116.21532	877		OP SALLY II MAY 90	−221	185	USMC/SIO
SAND	34.25500	−116.27888	833	EV4004	SAND HILL 1939 1981	−542	1	USGS/USGS
SCP1	34.26687	−116.00621	607		DEMO 2 SEP 98	−227	35	USMC/SIO
SCP2	34.41924	−115.96851	480	EU1185	SIGN 1935	−377	6	UCLA/SIO
SCP4	34.34839	−116.18636	579		BLADE 1973	−221	6	USMC/SIO
SCP5	34.43248	−116.23686	791		BRAVO-2	−377	6	UCLA/SIO
SCP6	34.40701	−116.34496	678	EV4002	MILL 1935	−377	6	UCLA/SIO
SIBE	34.62426	−116.01558	362		3056 S	−483	1	CWU/JPL
SILV	35.39699	−116.29126	610		none [Silver Lake]	−483	3	CWU/CWU
SOAP	34.90385	−116.98077	661	EV9241	HPGN 0804 GPS-SOAP 1990	−480	7	CADT/UCLA
STCH	34.63536	−116.31209	584		DEC STA STACHIA MAY 89	−229	186	USMC/UCLA
TROY	34.83860	−116.53054	613		3057 S	−483	1	CWU/JPL
XERO	34.26599	−116.02033	664		XEROX	−743	184	USMC/USC

Coordinates are ellipsoidal. "PID" is the permanent ID used as a designator by the National Geodetic Survey. "Last" is the number of days before the Hector Mine earthquake that the last pre-event measurement was made. "First" is the number of days after the earthquake that the first postseismic measurement was made. Institution acronyms are California Department of Transportation (CADT), Central Washington University (CWU), Jet Propulsion Laboratory (JPL), Massachusetts Institute of Technology (MIT), Scripps Institution of Oceanography (SIO), United States Geological Survey (USGS), United States Marine Corps (USMC), University of California, Los Angeles (UCLA), and the University of Southern California (USC). A downloadable version of this table is available through the Website *http://pasadena.wr.usgs.gov/hector/.*

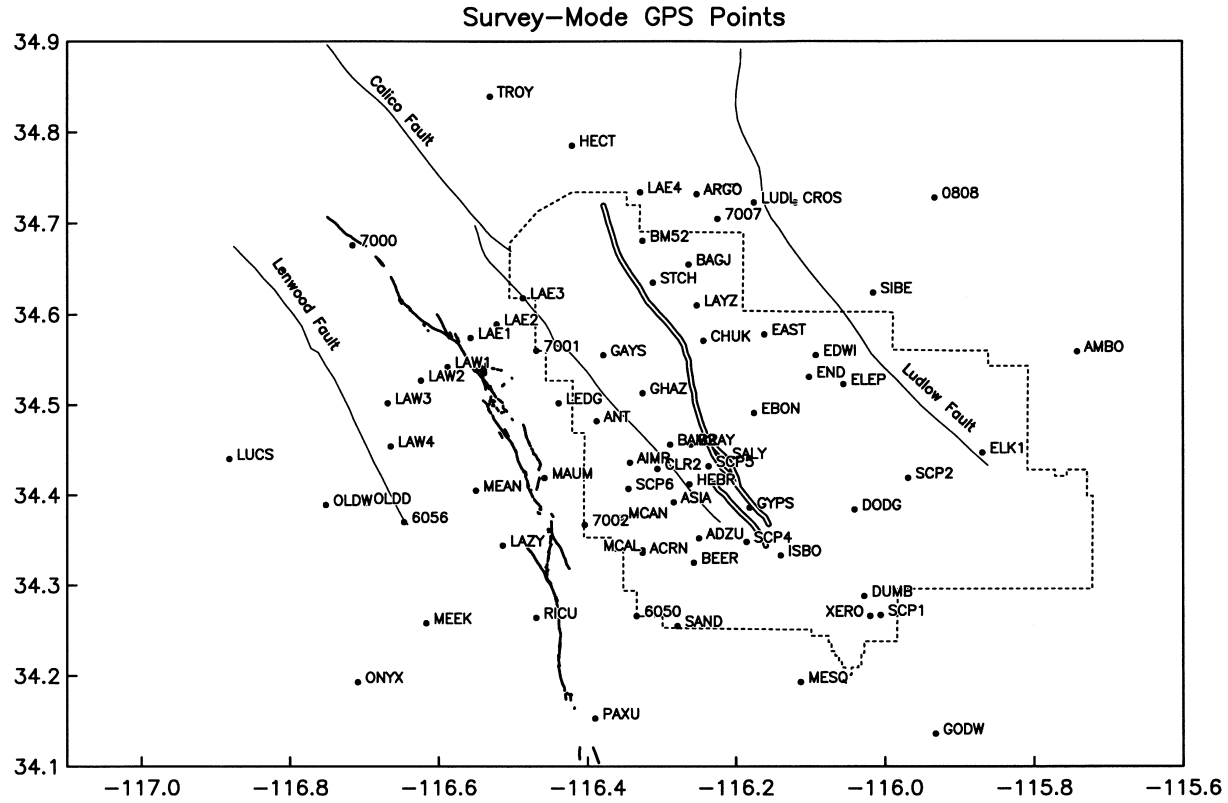

Figure 1. Survey-mode GPS stations in the vicinity of the Hector Mine rupture (shown as a double black line). The station codes are as used in Table 1 and Table 2. The dashed line marks the boundary of the USMC base, MCAGCC. The heavy black line shows the mapped rupture of the 1992 Landers earthquake; other active faults in the area are shown as light lines, and named.

to producing low errors for the final position estimates (though this was not always achieved).

We next used the GLOBK Kalman-filter package to combine the individual loose solutions and estimate station positions before and after the earthquake, all stations within 150 km being allowed to have an arbitrary offset at the time of the shock. The reference frame was provided by a tight constraint applied to the orbits and by the assumption of no motion for the more distant stations (MONP, BLYT, JPLM, VNDP, CMBB, and FARB). The SCIGN results indicate that none of these moved more than 1 cm at the time of the mainshock.

Interseismic Corrections

Fortunately, many sites were observed not too long before the mainshock, but some had not been observed in years, not since shortly after the 1992 Landers earthquake. We therefore applied a correction for the interseismic motion of these points; this correction includes both the usual secular part and long-term postseismic motions caused by the Landers shock. For some points there are sufficient data after Landers to estimate the interseismic velocity directly, but for many others (notably the USMC-observed stations) we lack such measurements.

The basis for our interseismic velocity estimates was an interim set of SCEC crustal motions (station velocities), produced by rotating velocities from three sources to a common reference frame (T. A. Herring, personal comm., 2001). The first source was a provisional update of the SCEC crustal motion map, using somewhat more stations than were included in Version 2 of the map; the second was an analysis of the SCIGN data; and the third was an analysis at MIT of the data described by McCluskey *et al.* (2001) The updated SCEC crustal motion map includes estimates for secular velocities of stations. In the Landers area this will of course include any long-term postseismic readjustments. For consistency with these, we excluded two sets of velocities from the Landers area: (1) the velocities deduced from electronic distance meter (EDM) data by Dong *et al.* (1998), which predate the Landers earthquake, and (2) the velocities at the SCIGN sites OAES and LDES, which are based largely on post–Hector Mine data. This meant that, in the immediate area of the Landers (and Hector Mine) earthquake, all available velocities were post-Landers; farther southwest, where the San Andreas fault affects the velocities more, some of the velocities are partly pre-Landers.

To get velocities at additional points, we interpolated the velocities to the locations of all points using a Gaussian weighting and local regression (fitting for a local velocity, with constant strain rate and spin) as in Shen *et al.* (1996). To remove possible outliers, we compared these interpolated velocities with those used as input; if the weighted difference exceeded three standard deviations, the velocity was not used. While this resulted in 80 out of 640 velocities being rejected overall, only 2 were rejected in the area covered by Figure 1. Finally, we interpolated the velocity to all points (including those used as input); the interpolation scheme also gave standard errors for each velocity. This interpolated velocity, multiplied by the time span in Table 1, gave the total interseismic correction, which (with its errors) is given in Table 2. For example, at station 7002, the estimated north velocity is 9.3 $\pm$ 0.8 mm/yr. Since the span between pre- and post–Hector Mine data was 7.49 years, this gives a correction of 69.7 mm to the offset of 273.7 mm between these epochs, for the final coseismic offset in Table 2 of 204.0 mm. At station LAZY, the interpolated north velocity was larger (15 mm/yr) but the time span less (1.33 years), so the correction is only 20 mm. Thus, the correction for interseismic motion is largest for stations closest to the San Andreas fault and for sites (such as 7002) with long time spans between the observations; in most cases it is less than a few centimeters.

Since many of the points were first observed within 6 days of the earthquake, this time is probably the best reference epoch to which our postearthquake measurements can be referred; this also corresponds to the date at which postearthquake interferometric synthetic aperture radar (InSAR) data are available. Most of the GPS data discussed here, like the InSAR data, thus include the effects of any immediate postseismic motion, as well as the dynamic rupture. The only points potentially requiring substantial correction for postseismic motion are those first observed in January and April 2000. However, the SCIGN data (Hudnut *et al.*, 2002) do not show displacements of more than about 3 cm over the first 6 months, only a small fraction of the displacements observed at these near-fault points.

Results

For each station, Table 2 gives the interseismic corrections, with our best estimate of the coseismic displacement; as explained previously, this estimate was found by combining the offset between the two epochs in Table 1 with the interseismic correction. Figures 2 through 4 plot these estimated coseismic offsets. Note that in Figure 2 the plotted displacements have been scaled in a somewhat unusual way: the length of each displacement vector is proportional to the cube root of the magnitude of the displacement, with the error ellipse for each vector scaled as the vector is. This nonlinear scaling reduces the range of vector lengths, and so makes it easier to see consistency (or the lack of it).

The horizontal data (Fig. 2) show a clear pattern, basically what would be expected from a finite fault with primarily strike-slip movement. The points closest to the central part of the fault (e.g., CHUK, GAYS, and GHAZ) show larger displacements than those closest to its southern part, indicating that more slip occurred at the northern part of the Bullion fault, consistent with the mapped surface offsets (Treiman *et al.*, 2002).

Possible vertical motions are of considerable importance in interpreting the InSAR data, since these would cause

Table 2
Coseismic Displacements

ID	N Disp	N Err	E Disp	E Err	Z Disp	Z Err	N Inter	Err	E Inter	Err
0803	−76.8	12.1	−46.4	16.0	21.1	63.7	3.3	4.1	−4.5	3.9
0808	−98.6	8.8	−10.5	9.1	31.8	22.6	2.4	4.7	0.9	4.9
6050	198.9	7.2	29.1	7.3	27.0	21.7	15.5	1.1	3.2	1.1
6056	37.4	6.7	−18.1	6.7	5.8	13.8	31.9	0.9	−13.2	0.9
7000	13.9	6.6	−196.2	6.6	−19.5	13.8	6.1	0.6	−6.3	0.6
7001	128.0	6.5	−267.8	6.5	−43.1	9.6	10.6	1.3	−7.3	1.3
7002	204.0	13.1	41.0	32.6	21.1	29.1	69.7	6.0	−8.2	6.7
7007	−759.5	44.8	−192.4	83.5	−105.8	237.7	17.4	8.0	−9.4	8.0
ACRN	317.6	26.8	−9.4	117.6	−87.4	100.5	8.1	1.3	0.4	1.3
ADZU	330.8	10.5	−65.8	14.7	−43.2	16.7	11.5	6.9	2.3	7.1
AIMR	629.0	11.5	61.9	35.6	−57.9	36.5	3.7	1.8	0.6	1.8
AMBO	−45.4	8.2	42.9	8.9	−11.2	13.3	0.8	4.8	3.8	5.1
ANT_	577.2	7.0	84.6	7.0	−73.7	17.2	5.4	1.4	−1.0	1.6
ARGO	−760.6	10.2	−285.5	27.2	−92.5	47.3	2.6	1.3	−1.7	1.3
ASIA	507.9	7.7	−43.4	7.5	−19.7	17.7	3.2	2.7	1.4	2.7
BAGJ	−1056.0	9.5	250.5	15.7	−22.0	48.1	3.5	1.5	−2.2	1.5
BAM2	990.9	17.3	−62.7	25.1	−146.2	30.6	6.1	5.9	2.0	5.9
BEER	318.9	15.2	23.2	53.8	−7.7	96.7	6.0	2.1	1.1	2.2
BM52	−1066.1	7.5	−166.3	7.8	−283.9	20.5	3.5	1.4	−2.8	1.4
BRAY	1018.9	8.7	−348.3	10.6	−10.6	38.7	4.1	2.4	0.8	2.4
CHUK	−1895.0	8.0	1070.0	8.3	298.3	28.7	3.0	1.1	−0.9	1.1
CLR2	639.1	17.0	−28.9	17.0	−56.7	19.1	16.2	15.5	8.1	15.5
CROS	−319.6	22.5	−64.7	38.9	27.7	75.2	4.3	3.8	−0.8	3.8
DODG	−163.8	7.8	386.2	7.4	−24.5	23.4	3.7	1.7	2.0	1.7
DUMB	−82.4	26.7	151.2	132.3	−12.3	157.9	3.9	2.0	2.6	2.0
EAST	−715.9	8.0	441.2	12.6	−76.9	27.6	3.9	1.5	−0.5	1.5
EBON	−821.7	7.0	634.9	6.8	57.2	15.3	5.0	1.7	0.8	1.7
EDWI	−335.7	70.1	365.4	100.4	1.3	307.0	3.4	1.4	0.9	1.4
ELEP	−227.9	48.2	350.0	187.5	27.6	291.8	3.3	1.5	1.7	1.6
ELK1	−73.6	13.2	149.3	72.7	−22.5	33.8	1.7	2.4	2.1	2.5
END_	−370.0	8.5	399.4	13.3	17.8	36.1	3.7	1.5	1.1	1.5
GAYS	696.0	13.9	−179.8	32.5	−186.3	28.0	9.0	3.2	−2.4	3.4
GHAZ	1217.1	27.7	87.9	46.7	−286.3	51.7	8.2	4.5	−0.4	4.5
GODW	−36.4	7.0	3.3	7.3	−7.8	20.8	4.8	1.3	3.3	1.3
GYPS	382.1	7.0	90.9	7.2	−29.9	10.0	4.5	2.4	2.0	2.4
HEBR	625.6	19.8	−63.1	99.1	−86.3	138.3	2.9	3.1	1.5	3.1
HECT	−38.1	6.5	−181.8	6.5	11.1	8.6	4.3	0.9	−4.4	0.9
ISBO	585.6	8.7	278.7	8.7	−203.7	16.9	10.7	5.4	4.3	5.4
LAE1	62.5	6.4	−230.9	6.3	−71.3	9.0	14.4	0.7	−12.1	0.7
LAE2	93.9	6.8	−293.0	6.9	−10.2	15.0	11.7	0.8	−10.5	0.8
LAE3	135.6	7.4	−443.8	9.6	14.6	24.7	9.2	0.8	−9.2	0.8
LAE4	−834.4	8.5	−279.8	10.9	−143.6	39.2	4.8	1.5	−4.1	1.5
LAW1	49.9	6.4	−143.3	6.2	−15.1	7.2	18.2	0.7	−13.4	0.7
LAW2	32.8	7.9	−120.8	13.4	−11.1	30.1	21.0	0.7	−14.9	0.7
LAW3	14.8	9.9	−93.2	10.4	6.1	46.3	24.3	0.7	−16.4	0.7
LAW4	23.8	9.6	−61.1	9.3	3.1	45.5	26.8	0.7	−15.4	0.7
LAYZ	−1215.8	20.8	1041.0	90.6	523.4	165.8	4.1	1.6	−1.9	1.6
LAZY	150.1	6.4	15.6	6.4	48.1	9.3	20.0	0.8	−5.6	0.8
LEDG	324.7	7.0	−12.5	6.9	−13.3	16.1	11.6	1.5	−4.4	1.7
LUCS	2.7	32.1	−148.2	77.1	−59.7	168.5	28.0	1.2	−21.4	1.2
LUDL	−445.0	47.4	−238.3	139.0	−84.8	160.5	5.1	3.1	−1.8	3.1
MAUM	250.0	7.3	66.2	7.2	5.8	18.2	17.8	1.2	−5.0	1.3
MCAL	279.9	13.0	−66.4	35.6	−99.8	21.5	18.2	3.1	1.0	3.3
MCAN	393.6	12.6	21.4	40.9	−47.9	43.0	7.1	1.3	0.2	1.3
MEAN	123.8	7.9	−8.2	7.7	22.5	27.5	25.4	0.8	−9.7	0.8
MEEK	35.9	6.9	3.1	6.8	7.5	13.7	32.5	1.5	−8.4	1.9
MESQ	27.9	6.9	1.0	6.9	7.3	13.5	9.7	2.1	4.4	2.1
OLDD	25.1	6.5	−32.8	6.5	3.9	11.8	30.1	0.7	−15.0	0.9
OLDW	6.3	6.5	−34.5	6.4	−5.0	11.6	28.2	0.8	−15.5	0.8
ONYX	58.3	7.4	−46.2	8.6	24.1	21.8	5.8	0.3	−1.7	0.3
PAXU	76.1	26.7	10.6	67.7	−15.4	129.3	20.1	1.5	3.9	1.5

(*continued*)

Table 2
Continued

ID	N Disp	N Err	E Disp	E Err	Z Disp	Z Err	N Inter	Err	E Inter	Err
RAIN	−17.4	6.5	−60.9	6.4	16.7	7.9	18.1	1.2	−8.8	1.2
RICU	142.0	6.5	1.7	6.5	84.8	10.6	22.8	1.4	−1.9	1.4
RVAL	−37.6	6.5	−32.4	6.5	22.4	9.1	0.0	1.3	0.0	1.3
SALY	−42.4	7.3	15.7	7.4	358.9	19.1	4.7	1.9	1.2	1.9
SAND	190.3	6.5	12.8	6.4	−10.8	7.5	9.2	0.9	3.8	1.0
SCP1	−73.1	6.5	108.3	6.6	9.4	9.8	2.4	1.3	1.9	1.3
SCP2	−111.9	7.5	280.0	17.6	−7.4	14.8	2.5	1.7	1.9	1.7
SCP4	385.0	6.9	60.0	6.9	−28.6	13.6	2.6	1.7	0.9	1.7
SCP5	828.3	7.2	−263.5	7.4	−84.6	15.9	4.0	2.1	1.2	2.1
SCP6	519.9	6.9	42.6	7.0	−12.0	9.4	4.6	1.5	0.5	1.6
SIBE	−169.8	6.5	107.4	6.3	6.5	7.1	2.4	1.3	1.2	1.3
SILV	−36.5	6.7	−40.0	7.0	5.4	8.8	−3.7	1.9	0.3	1.9
SOAP	−7.5	6.5	−70.2	6.5	−5.9	9.7	15.7	1.1	−8.6	1.1
STCH	−1110.8	7.9	463.3	8.9	−173.9	24.8	3.9	1.8	−2.5	1.8
TROY	24.7	6.5	−156.2	6.3	−4.3	7.4	5.7	1.3	−5.8	1.3
XERO	−77.0	30.6	108.7	58.0	−157.9	99.0	8.9	4.3	6.8	4.3

The first six numerical columns give the estimated offsets and their errors, after applying the correction for interseismic displacement between the last pre- and first post–Hector Mine measurement; these corrections are in the last four columns (there is no correction to the vertical displacements). A downloadable version of this table is available through the Web site *http://pasadena.wr.usgs.gov/hector/*.

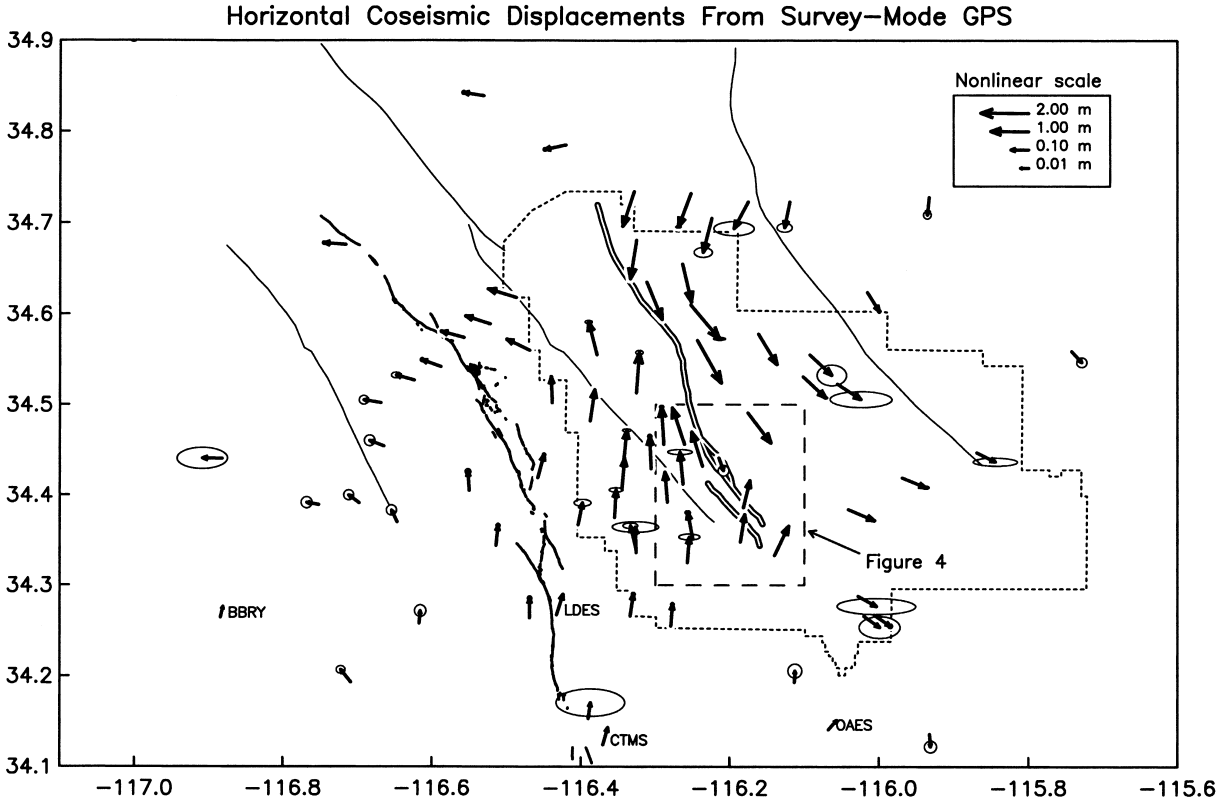

Figure 2. Estimated horizontal coseismic displacements of survey-mode GPS stations, including the correction for interseismic motion. Note that directions are true, but arrow lengths scale as the cube root of the total displacement. Error ellipses indicate 95% confidence. The long-dashed line marks the boundary of Figure 4. The four named sites are the SCIGN stations which were operating in this region; for these the coseismic displacement comes from the report of the SCIGN Analysis Committee (1999). The faults and MCAGCC boundary are as in Figure 1.

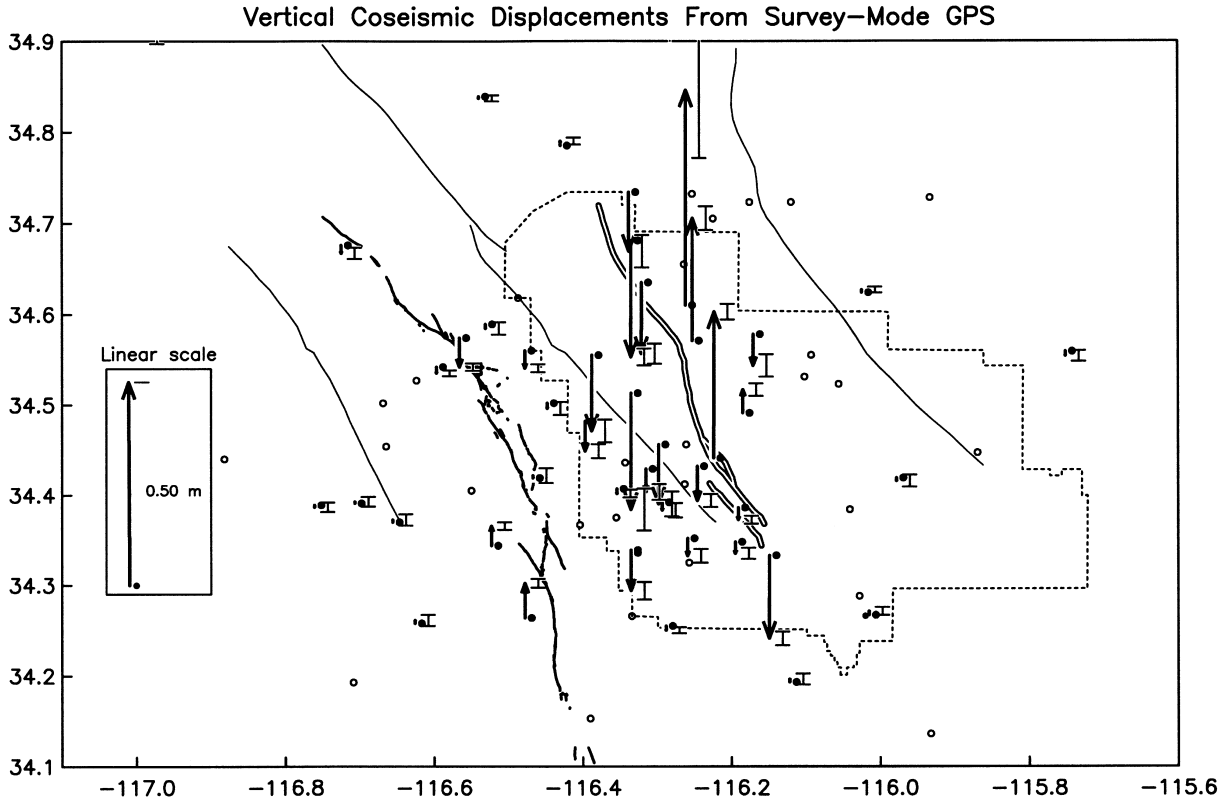

Figure 3. Estimated vertical coseismic displacements of survey-mode GPS stations, for all cases in which the displacement exceeded twice the standard error, or this error was less than 20 mm. For each point, the arrow showing displacement is plotted just to the left of the station, and the error bar is plotted just to the right, next to the tip of the arrow. The faults and MCAGCC boundary are as in Figure 1.

changes in the line-of-sight direction that could be misinterpreted as large horizontal motions. Figure 3 shows some of the vertical results; unfortunately, because of the relatively short observation spans of the pre–Hector Mine data, the vertical errors for many sites are large. In agreement with the InSAR results of Fialko *et al.* (2001), the sites near the central part of the fault show upward motion to the northeast of the rupture, and downward to the southwest, and along the northernmost part of the rupture, downward motion to the northeast. Most far-field sites show little vertical motion, with the exception of a few that are relatively close to the 1992 Landers rupture.

One station that shows large vertical motion is a rather unusual case: station SALY, located between two mapped ruptures of the Bullion fault. Figure 4 shows a detail of the area around this point: it is evident that stations on either side of the two ruptures moved oppositely, as expected, with SALY, (on the block between the ruptures) moving very little horizontally but rising by about 0.3 m. This point is located on the crest of a small hill.

Conclusions

The number of points at which offsets could be determined for the Hector Mine earthquake makes this one of the geodetically better observed events of its size anywhere—somewhat surprisingly, given its location in a nearly unpopulated desert region. This underscores a point which was first made evident by the Loma Prieta earthquake: GPS techniques have such high inherent precision that even data collected for nonscientific purposes can be useful for determining coseismic offsets, and such data are becoming increasingly widespread with the increasing use of GPS. It seems likely that for many future earthquakes survey-mode data not collected for scientific purposes will be an important source of closely spaced measurements of offsets; the challenge will be finding such data from the many available surveys.

Even the relatively large number of points shown in Figure 2 is nowhere near the uniformly dense coverage provided by InSAR. Determining the relative importance of GPS

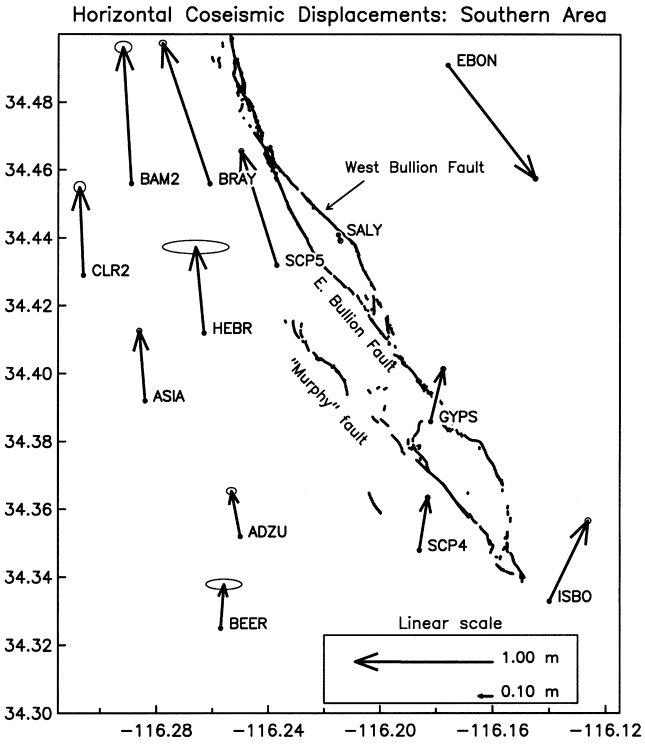

Figure 4. Detail of Figure 3, showing the southern part of the fault, with the rupture shown in full detail (heavy lines), and the horizontal displacements plotted with linear scaling. Error ellipses indicate 95% confidence. Note the very small displacement at SALY, between the two mapped ruptures.

and InSAR data is beyond the scope of this paper, as it would require a systematic inversion for fault slip. Given the very high coherence available for InSAR images of this earthquake, and the availability of along-track and cross-track data, the Hector Mine event is likely to represent a best case for InSAR, with full vector data being recoverable (Fialko *et al.*, 2001; Sandwell *et al.*, 2002). However, the GPS and InSAR data probably remain complementary, given the much higher precision of the former in the horizontal, as well as its immunity to long-wavelength biases.

Acknowledgments

It will be evident that without the efforts of many members of the U.S. Marine Corps, we would have had much less to write about. Our primary thanks go to CWO5 Alan Matthews, Sgt. Mulson, and Sgt. J. E. Price, Meteorology and Survey Section, 11th Marine Artillery Regiment, for allowing us the use of the 1997 and 1999 surveys, and providing us with copies of the data and logsheets. We also thank Lt. Col. J. Tabak and Mr. Paul "Kip" Otis-Diehl of MCAGCC for facilitating our visits to the base, the staff of BearMAT for keeping track of us, and especially W. Karl Gross (USGS, and formerly USMC) for coordinating access to the base. We thank Andrea Donnellan, Mark Smith, and Ken Hurst for their efforts in installing and maintaining the TROY and SIBE receivers. We also acknowledge the efforts of Mr. Stanley Cindrity (UCLA) for getting measurements inside MCAGCC in 1998. We thank Don Elliot, Michelle Smith, Steve Bralla, Chengkun Zhao, Yufang Rong, Youlin Chen, Hanbiao Wang, Min Wang, Zhen Liu, John Galetzka, and Matt Van Domeselaar for their help in the field; Dave Jackson for his support in organizing surveys in the Landers area; Bob King and Simon McCluskey for their patient help during our processing of the data; and Ken Hudnut, Meghan Miller, and Dave Sandwell for their advice and assistance. We especially thank Tom Herring for providing us with the interseismic velocity information. Support for this work came primarily from the Southern California Earthquake Center, which is funded by NSF Cooperative Agreement EAR-8920136 and USGS Cooperative Agreements 14-08-0001-A0899 and 1434-HQ-97AG01718, and also from USGS grant 98-HQ-GR1015. CWU's research in this area has been supported by NASA through the Dynamics of the Solid Earth program. The SCEC contribution number for this paper is 614.

References

Agnew, D. C., and K. Sieh (1978). A documentary study of the felt effects of the great California earthquake of 1857, *Bull. Seism. Soc. Am.* **68,** 1717–1729.

Dong, D., T. A. Herring, and R. W. King (1998). Estimating regional deformation from a combination of space and terrestrial geodetic data, *J. Geodesy* **72,** 200–214.

Fialko, Y., M. Simons, and D. Agnew (2001). The complete (3-D) surface displacement field in the epicentral area of the 1999 M_w 7.1 Hector Mine earthquake, California, from space geodetic observations, *Geophys. Res. Lett.* **28,** 3063–3066.

Hayford, J. F., and A. L. Baldwin (1908). Geodetic measurements of earth movements, in *The California Earthquake of April 18, 1906*, A. L. Lawson (Editor), Carnegie Institution of Washington, Washington, DC, 114–145.

Herring, T. (2001). Global Kalman filter VLBI and GPS analysis program, version 5.0, Internal Report, Massachusetts Institute of Technology, Cambridge Massachusetts.

Hudnut, K. W., Y. Bock, M. Cline, P. Fang, Y. Feng, J. Freymueller, X. Ge, W. K. Gross, D. D. Jackson, M. Kim, N. E. King, J. O. Langbein, S. C. Larsen, M. Lisowski, Z.-K. Shen, J. L. Svarc, and J. Zhang (1994). Coseismic displacements of the 1992 Landers earthquake sequence, *Bull. Seism. Soc. Am.* **84,** 625–645.

Hudnut, K. W., N. E. King, J. Galetzka, K. F. Stark, J. A. Behr, A. Aspiotes, S. vanWyk, S. Dockter, and F. Wyatt (2002). Continuous GPS observations of postseismic deformation following the 16 October 1999 Hector Mine earthquake (M_w 7.1), *Bull. Seism. Soc. Am.* **92,** 1403–1422 (this issue).

Hudnut, K. W., Z. Shen, M. Murray, S. McClusky, R. W. King, T. Herring, B. Hager, Y. Feng, P. Fang, A. Donnellan, and Y. Bock (1996). Coseismic displacements of the 1994 Northridge, California, earthquake, *Bull. Seism. Soc. Am.* **86,** S19–S36.

Hurst, K. J., D. F. Argus, A. Donnellan, M. B. Heflin, D. C. Jefferson, G. A. Lyzenga, J. W. Parker, M. Smith, F. H. Webb, and J. F. Zumberge (2000). The coseismic geodetic signature of the 1999 Hector Mine earthquake, *Geophys. Res. Lett.* **27,** 2733–2736.

King, R. W., and Y. Bock (2001). Documentation for the GAMIT GPS analysis software, Internal Report, Massachusetts Institute of Technology and University of California, San Diego.

McClusky, S. C., S. C. Bjornstad, B. H. Hager, R. W. King, B. J. Meade, M. M. Miller, F. C. Monastero, and B. J. Souter (2001). Present day kinematics of the Eastern California Shear Zone from a geodetically constrained block model, *Geophys. Res. Lett.*, **28,** 3369–3372.

Miller, M. M., D. P. Johnson, T. H. Dixon, and R. K. Dokka (2001). Refined kinematics of the Eastern California Shear Zone from GPS observations, 1993–1998, *J. Geophys. Res.* **106,** 2245–2263.

Sandwell, D. T., L. Sichoix, D. Agnew, Y. Bock, and J.-B. Minster (2000). Near real-time radar interferometry of the M_w 7.1 Hector Mine earthquake, *Geophys. Res. Lett.* **27,** 3101–3104.

Sandwell, D. T., L. Sichoix, and B. Smith (2002). The 1999 Hector Mine

earthquake, Southern California: vector near-field displacements from ERS InSAR, *Bull. Seism. Soc. Am.* **92,** 1341–1354 (this issue).

Savage, J. C., and J. L. Svarc (1997). Postseismic deformation associated with the 1992 M_w 7.3 Landers earthquake, Southern California, *J. Geophys. Res.* **102,** 7565–7577.

Scientists of the U.S. Geological Survey, the Southern California Earthquake Center, and the California Division of Mines and Geology (2000). Preliminary report on the 16 October *M* 7.1 Hector Mine, California, earthquake, *Seism. Res. Lett.* **71,** 11–21.

SCIGN Analysis Committee (1999). Hector Mine earthquake coseismic displacement comparison. *http://pasadena.wr.usgs.gov/office/nking/AnalysisComm/HectorComparison.html* (last accessed February 2002).

Shen, Z.-K., D. Jackson, Y. Feng, M. Cline, M. Kim, P. Fang, and Y. Bock (1994). Postseismic deformation following Landers earthquake, California, June 28, 1992, *Bull. Seism. Soc. Am.* **84,** 780–791.

Shen, Z.-K., D. D. Jackson, and B. X. Ge (1996). Crustal deformation across and beyond the Los Angeles basin, *J. Geophys. Res.* **101,** 27,957–27,980.

Treiman, J. A., K. J. Kendrick, W. A. Bryant, T. K. Rockwell, and S. F. McGill (2002). Primary surface rupture associated with the M_w 7.1 16 October 1999 Hector Mine earthquake, *Bull. Seism. Soc. Am.* **92,** 1171–1191 (this issue).

Institute of Geophysics and Planetary Physics
Scripps Institution of Oceanography
University of California, San Diego
La Jolla, California 92093-0225
(D.C.A., G.A., H.J.)

Department of Earth Sciences
University of Southern California
Los Angeles, California 90089-0740
(S.O.)

Department of Earth and Space Sciences
University of California, Los Angeles
Los Angeles, California 90024-1567
(Z.-K.S.)

U.S. Geological Survey
Menlo Park, California 94025
(J.S.)

Department of Geology
Central Washington University
Ellensburg, Washington 98926
(K.E.A.)

Earth Resources Laboratory
Massachusetts Institute of Technology
Cambridge, Massachusetts 02142-1324
(R.R.)

Manuscript received 14 February 2001.